Stretchable Spin Valve with Stable Magnetic Field Sensitivity by Ribbon-Patterned Periodic Wrinkles

Huihui Li, Qingfeng Zhan,* Yiwei Liu, Luping Liu, Huali Yang, Zhenghu Zuo, Tian Shang, Baomin Wang, and Run-Wei Li*

Key Laboratory of Magnetic Materials and Devices & Zhejiang Province Key Laboratory of Magnetic Materials and Application Technology, Ningbo Institute of Materials Technology and Engineering, Chinese Academy of Sciences, Ningbo 315201, People's Republic of China

Supporting Information

ABSTRACT: **A strain-relief structure by combining the strain-engineered periodic wrinkles and the parallel ribbons was employed to fabricate flexible dual spin valves onto PDMS substrates in a direct sputtering method. The strain-relief structure can accommodate the biaxial strain accompanying with stretching operation (the uniaxial applied tensile strain and the induced transverse compressive strain due to the Poisson effect), thus significantly reducing the influence of the residual strain on the giant magnetoresistance (GMR) performance. The fabricated GMR dual spin-valve sensor exhibits the nearly unchanged MR ratio of 9.9%, magnetic field sensitivity up to 0.69%/Oe, and zero-field resistance in a wide range of stretching strain, making it promising for applications on a conformal shape or a movement part.**

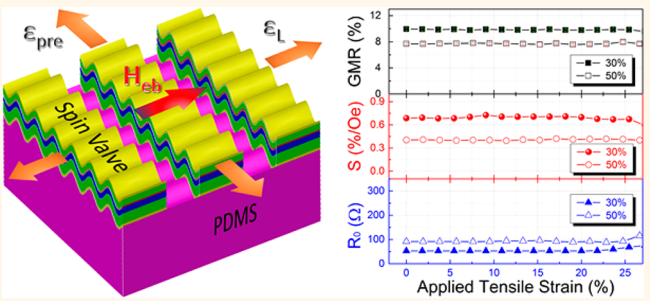

KEYWORDS: *stretchable, magnetoelectronics, GMR spin valve, strain engineering, wrinkle*

Flexible electronics possess tremendous advantages in manufacturing cost, processing efficiency, and wearable application over their conventional silicon-based counterparts.[1−4] They have driven the prevalence of the wearable devices such as mobile gadgets and healthcare sensors. Meanwhile, the wearable applications are in turn driving the flexibilization of the well-developed magnetoelectronic components,[3,5−14] which are supposed to be increasingly stretchable, conformally shapeable, light-weighted, *etc*. As an indispensable part of the flexible spintronics devices family, giant magnetoresistance (GMR) based flexible magnetic sensor, which is very sensitive to external magnetic field and can be communicated wirelessly, has attracted a lot of attention recently.

Instead of the conventional rigid silicon-integrated circuit, a key architecture to achieve a desired flexibility in GMR sensors is to install the GMR multilayer onto flexible substrates *via* direct coating or multistep transfer.[5−10,13,15−17] However, for this vastly utilized metal/polymer architecture, there are great disparities in the intrinsic elastic properties of functional magnetic layers and polymer substrates, *e.g.*, the stretching limit is less than 1% for metal, but a few percent for plastics, and more than 100% for elastomer. The mismatch of the elasticity causes two critical issues that need to be addressed for flexible magnetoelectronics: (i) the limited stretchability due to the fragile nature of the magnetic thin film, and (ii) the unstable magnetic field sensitivity due to the large residual strain.[6,10,13,16,17] For instance, Chen *et al.* fabricated a GMR structure of Co/Cu multilayers on a photoresist-buffered plastic substrate and even better GMR values than those on silicon substrates were achieved. The GMR ratio and the magnetic field sensitivity were varied under bending strains of a few percent due to the change of the Cu spacer thickness.[6] Melzer *et al.* demonstrated a highly stretchable spin valve sensor, which shows a stable GMR magnitude during stretching, by means of the predetermined periodic fractures and random wrinkling on the superelastic poly(dimethylsiloxane) (PDMS) substrate. It was found that with rising strain the sample resistance and the magnetic field sensitivity are increased and decreased, respectively, due to the irregular cracking structure and the induced shape anisotropy.[13] The experimental and theoretical works have shown that the applied strain can tune the magnetization orientation of the ferromagnetic layers in a spin valve *via* the inverse magnetostrictive effect and significantly destabilize its GMR performance.[16,18−27] Therefore, how to

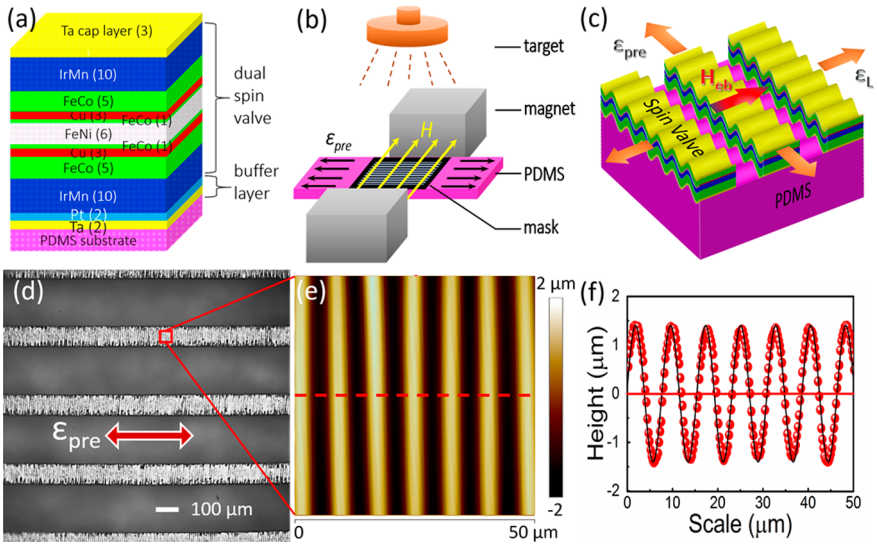

Figure 1. (a) The layer structure of the dual spin valve (not to scale); (b) an illustrative drawing of the experimental setup for the sample fabrication; (c) an schematic diagram for the appearance of as-fabricated sample after releasing the tensile prestrain; (d) optical image of the as-fabricated SVR-30%; (e) the surface topography and (f) the cross-sectional view extracted along the red dashed line of SVR-30% by AFM (red dots, measured results; black line, sinusoidal fitting).

simultaneously achieve a desired stretchability and a stable magnetic field sensitivity with strain is still a great challenge for flexible magnetic sensors.

In recent years, artificial wrinkling structures, which can be repeatedly stretched and then fully recovered, have been widely adopted in fabricating different stretchable electronics, such as field effect transistor, integrated circuits, organic light-emitting diodes, supercapacitors, *etc.*[12,13,28−36] Most recently, Melzer *et al.* fabricated an ultrastretchable wrinkled GMR sensor by transferring the GMR multilayer onto a prestrained elastic substrate and capsulating it by thin polyethylene terephthalate (PET) film. The strain-engineered wrinkles significantly promote the stretchability and the strain stability of the GMR sensor.[37] In this study, we employed a strain-relief architecture based on the strain-engineered wrinkles to fabricate flexible magnetoelectronics. The architecture is composed of both self-assembled periodic wrinkles and parallel ribbons and can be realized simply by direct sputtering with metal mask on prestrained PDMS substrates. In this structure, the biaxial strain accompanying with stretching operation (the uniaxial applied tensile strain and the induced transverse compressive strain due to the Poisson effect) can be accommodated, thus significantly reducing the influence of the residual strain on the GMR performance. Moreover, we employ a dual spin valve structure, which has been demonstrated to show the higher GMR ratio and higher magnetic field sensitivity than those of the conventional simple spin valve because of the spin dependent scattering on the both sides of the free layer,[38−41] to construct the multilayer magnetic sensor. Different to the GMR multilayer-based magnetic sensor, the dual spin-valve sensor is appropriate for detecting weak field with high magnetic field sensitivity. The strain stability of GMR performance also benefits from the symmetric dual spin valve structure, where the magnetic free layer and the Cu spacer layer are located in the center of the film with nearly zero bending strain. Finally, an almost constant GMR ratio of 9.9%, a rather stable magnetic field sensitivity of 0.69%/Oe, and the nearly unchanged zero field resistance were obtained under a tensile stretch up to ~25%, making the strain-relief structure a promising architecture for manufacturing fully flexible electronics.

RESULTS AND DISCUSSION

The dual spin valve has a multilayer structure of IrMn (10 nm)/FeCo (4 nm)/Cu (3 nm)/FeCo (1 nm)/FeNi (6 nm)/FeCo (1 nm)/Cu (3 nm)/FeCo (4 nm)/IrMn (10 nm) and Ta buffer/capping layers (Figure 1a). As schematically illustrated in Figure 1b and Figure S1c of the Supporting Information, the dual spin valves were sputtering deposited on PDMS substrates with a series of uniaxial tensile prestrains (ε_{pre} = 0, 30% and 50%). A band-like shadow mask with a gap-to-gap distance (W_{PDMS}) of 200 μm and a gap width (W_{SVR}) of 100 μm was applied along the prestrain direction to obtain a ribbon-patterned structure. For reference, a continuous spin valve thin film was fabricated with a tensile prestrain of 30% but without a ribbon mask. Figure 1c shows a schematic drawing of the as-fabricated wrinkled spin valve ribbons (SVR), where the direction of the well-defined periodic wrinkles is perpendicular to the ribbons and parallel to the exchange bias. According to the Poisson effect, as the prestrain is released, the PDMS substrate displays an elongation ε_L in the lateral direction (perpendicular to the prestrain), which can be written as $\varepsilon_L = \nu_{PDMS}\varepsilon_{pre} = 0.5\varepsilon_{pre}$, where ν_{PDMS} = 0.5 is the Poisson ratio of PDMS.[42] Accordingly, the lateral tensile strains in the 30% and 50% prestrained thin films are 15% and 25%, respectively, which by far exceed the stretching limit of metallic thin films. Consequently, as a reference shown in Figure S2a of the Supporting Information, the film fabricated without the ribbon mask seriously cracks along the prestrain after releasing the prestrain. Therefore, the lateral tensile strain by the Poisson effect is devastating and should be avoided during the fabrication. In contrast, cracks are not observed in the measurement range up to 3 × 3 mm^2 in both SVR samples fabricated with the 30% and 50% prestrains (SVR-30% and SVR-50%). They exhibit a uniform wavy structure over a large area of a few square centimeters (Figure 1d). This is because most of the induced lateral tensile strain by the Poisson effect is

released through the bared PDMS area where is much softer than that covered by the metallic multilayers.

As respectively shown in Figure 1e and Figure S2c of the Supporting Information, the surface topographies of both SVR-30% and SVR-50% characterized by atomic force microscope (AFM) exhibit ordered wrinkled patterns. The cross-sectional profile of these wrinkles can be well fitted to a sinusoidal curve. A wavelength of λ = 7.66 μm and an amplitude of A = 1.42 μm are obtained for the SVR-30% (Figure 1f). As for the sample of SVR-50%, the fitted wavelength and amplitude increase to 8.22 and 1.75 μm, respectively (Supporting Information, the inset of Figure S2c). The wavelength and amplitude in such a wrinkled geometry agree well with the nonlinear elastic solution for wrinkling,[30,31,43,44] which indicates that the strain-engineered wrinkles in SVRs are elastic deformations and therefore are reversible. The mechanical stretchability of the as-fabricated SVR-50% was tested by applying a tensile strain along the prestrain direction. Optical images in Figure 2a show the evolution of the SVRs' topography and the corresponding fast Fourier transforms (FFT) with increasing applied tensile strain. The information about periodicity (wavelength) of the SVR in the real space is simply reduced to a set of bright spots in the frequency space. The first order spot, whose distance to center is inversely proportional to the wavelength, is circled in red. As seen, their wavelength is almost constant when the tensile strain increases from 0 to 40%. When the applied tensile strain approaches and exceeds the prestrain, the wavelength gradually increases due to the plastic deformation of the metallic SVRs (see the FFT images for the cases of 50% and 60% applied stains). In addition, the image contrast between the wrinkle peak and the wrinkle trench is lowered with increasing applied tensile strain, reflecting that the wrinkles are flattened by the tensile stretching. In case of the applied tensile strain less than the prestrain, SVRs remain continuous and the wrinkling structure can be reversibly changed. When the applied tensile strain is smaller than the prestrain, the SVRs exhibit a good continuity with a nearly constant wavelength of 8.2 μm (Figure 2b). On the basis of the elastic model by Rogers *et al.*,[30,31] the wavelength of the sinusoidal wrinkle geometry can be solved by minimizing the total strain energy consisting of the bending strain energy and the stretching strain energy. The results can be written as below:

$$\lambda = \frac{\pi t}{\sqrt{\varepsilon_c}}$$

where

$$\varepsilon_c = 0.52\left[\frac{E_{sub}(1-\nu_f^2)}{E_f(1-\nu_{sub}^2)}\right]^{2/3}$$

is the critical strain beyond which wrinkle happens, and t is the film thickness of the rigid skin. ν is the Poisson ratio. E is the Young's modulus. The subscripts sub and f denote the soft substrate and the rigid skin film, respectively. Obviously, the wrinkle wavelength is only a function of the film thickness and the film/substrate modulus ratio and is independent of the strain state of the film. With this equation, the theoretical wavelength for this experiment is predicted at 7.96 μm even under different applied strains (Figure 2b). The following values have been taken for fitting: t = 50 nm, $\nu_f \approx 0.3$ for metal films, $\nu_{sub} \approx 0.5$ for PDMS membranes, E_f is estimated as the weighted average of the Young's moduli of all metallic layers and is about 200 GPa, and E_{sub} is measured to be 3.4 ± 0.1 MPa by a Peak-Force AFM. As seen, in the elastic deformation region of 0−50%, the experimental wavelength agrees well with the fitting results. The wavelength deviates seriously from the fitted straight line when the applied tensile strain is beyond the growth prestrain of 50%, where the fractures in the ribbons start to occur. One can conclude that the mechanical stretchability of wrinkled SVRs is roughly equal to the prestrain and hence can be preset by changing the prestrain during the film deposition.

The GMR performance of the wrinkled SVRs fabricated under various prestrains was measured by the standard four-wire method with an in-plane magnetic field applied perpendicular to the long axis of SVRs, *i.e.*, parallel to the exchange bias (the inset of Figure 3c). All samples show the typical dual spin valve GMR behaviors, where the GMR curves exhibit three resistance states due to the incoherent magnetic switching of the top and bottom pinned layers (indicated by arrows in Figure 3a).[41] The GMR ratios $(\Delta R/R_0)_{max}$ of 9.8%, 10.2%, and 7.9% are obtained in the spin valves of SVR-0%, SVR-30%, and SVR-50%, respectively (Figure 3a−c). The strain effect on the GMR performance of the wrinkled SVRs was measured by applying different tensile strains varying from

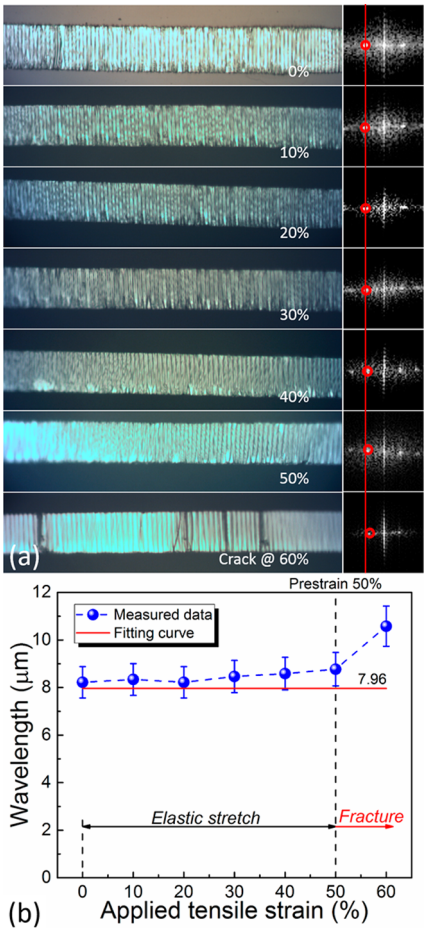

Figure 2. (a) The strain-dependent microstructure evolution of SVR-50% captured by an optical microscope (W_{SVR} = 100 μm). The corresponding FFT images are shown on the right side. (b) The dependence of the wrinkle wavelength on the applied tensile strain for the sample SVR-50%. The measured data is extracted from panel a. The red line is the fitting results based on the model by Rogers *et al.*[30,31]

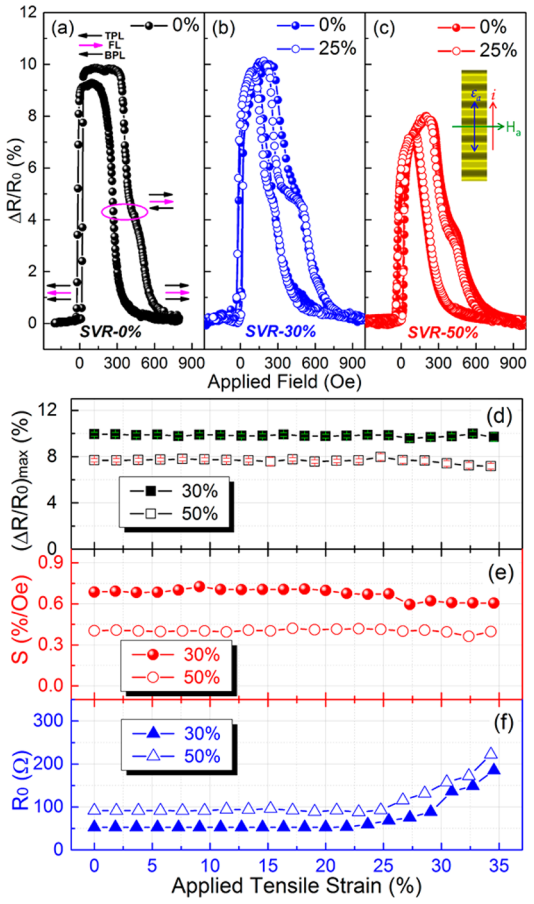

Figure 3. GMR curves of (a) SVR-0% without applied strain (the switching of magnetic layers indicated by arrows from top to bottom: top pinned layer-TPL, free layer-FL, and bottom pined layer-BPL), (b) SVR-30% with 0 (solid circles) and 25% (open circles) applied tensile strain, and (c) SVR-50% with 0 (solid circles) and 25% (open circles) applied tensile strain. The magnetic switching processes in (b) and (c) are similar to those in (a). Inset in (c) shows the GMR measurement geometry: both the current and the applied tensile strain are parallel to the ribbons, while the magnetic field is applied perpendicular to the ribbons. The applied tensile strain dependence of (d) the GMR ratio $(\Delta R/R_0)_{max}$ (squares), (e) the magnetic field sensitivity S (circles), and (f) the zero-field resistance R_0 (triangles) for SVR-30% (solid symbols) and SVR-50% (open symbols). The uniaxial tensile strain from 0 to 35% is applied along the ribbons.

a few percent to a few tens of percent parallel to the prestrain. The sample of SVR-0% grown without prestrain is very brittle and cracks seriously under an applied tensile strain even less than 2%, and the GMR signal becomes noisy (Supporting Information, Figure S3). In a stark contrast, for either the periodically wrinkled SVR-30% or SVR-50%, when applying a tensile strain of 25%, the measured GMR curves are almost unchanged (Figure 3b,c), signifying that the GMR performance of the wrinkled SVRs is insensitive to the stretching operation. The GMR ratio ($(\Delta R/R_0)_{max}$), the magnetic field sensitivity (S), and the zero-field resistances (R_0) of both SVR-30% and SVR-50% are plotted in Figure 3d–f. Here, the sensitivity S is defined as $\frac{1}{R_0}\frac{dR}{dH}\Big|_{d^2R/dH^2=0}$, where R and H are the measured sample resistance and the applied magnetic field, respectively. For the SVR-30%, the $(\Delta R/R_0)_{max}$ of 9.9%, the S of 0.69%/Oe, and the R_0 of 53 Ω are almost constant as increasing the applied tensile strain from 0 to 25%. In previous works, when stretching a magnetic sensor, the strain-induced magnetic anisotropy in the magnetic layer due to the inverse magnetostrictive effect significantly deteriorated its magnetic field sensitivity.[6,13] However, in our case, the large stretching tensile strain and the induced lateral compressive strain are released through the combined periodic wrinkling and parallel ribbon structures. The residual strain in the magnetic layer is negligible, and therefore, a constant magnetic field sensitivity can be achieved during stretching the SVRs. With further increasing the applied tensile strain beyond 25%, the GMR ratio and the magnetic field sensitivity become a little fluctuating. However, the zero field resistance continues to increase with rising tensile strain. The SVR-50% displays a similar strain dependent behavior as the SVR-30%. The almost constant GMR ratio of 7.9%, the magnetic field sensitivity of 0.4%/Oe, and the zero field resistance of 92 Ω are achieved in the tensile strain range of 0–25% (Figure 3d–f). It is found that the onset points for the distinct increase of the zero field resistance and the obvious fluctuations of the GMR ratio and the magnetic sensitivity in both SVR-30% and SVR-50% are roughly superimposed at a tensile strain of ~25%. We ascribe this deterioration of GMR performance to the destabilization of wire contact at the high strain state (see Methods section for details). As a result, especially for the sample of SVR-50%, the experimentally observed stretchability is lower than our expectation that the stretchability should be close to the prestrain.

To assess the stretching fatigue of the wrinkled SVRs, we conducted two sequential cyclic stretching tests on the sample of SVR-30%. Each test comprises 500 stretching-releasing cycles, in which uniaxial tensile strains in a sequence of 0 → 10% → 0 (first test) or 0 → 20% → 0 (second test) along the prestrain direction are applied to the sample. The selected strain loadings (10% and 20%) are below the stretching limit of SVR-30%, and therefore, a stable GMR output during the stretching tests is expected. The GMR properties were recorded every 10 cycles. Nearly constant $(\Delta R/R_0)_{max}$, S, and R_0 are achieved around 9.9%, 0.69%/Oe, and 55 Ω, respectively, for both $(0 \rightarrow 10\% \rightarrow 0)_{500}$ and $(0 \rightarrow 20\% \rightarrow 0)_{500}$ tests (the subscript 500 indicates the total number of stretching cycles, Figure 4). For 0 → 10% → 0 cyclic test, the standard deviations of $(\Delta R/R_0)_{max}$, S, and R_0 are 1.4%, 2.6%, and 5.5%, respectively, revealing an excellent stability of the GMR performance during at least hundreds times of stretching-releasing cycles. As for 0 → 20% → 0 cycles, the corresponding standard deviations slightly increase to 2.0%, 3.5%, and 6.4%. The increased fluctuations should be correlated with the fatigue of electrodes. The stability of the magnetic field sensitivity under mechanical strains is a critically important parameter to evaluate the performance of a flexible magnetic sensor. On the basis of the strain-relief structure by combining the wrinkles and ribbons, we have achieved a stable magnetic field sensitivity over a wide range of applied tensile strain (from 0% to 25%), and the sensitivity exhibits a very small standard deviation of 2.6% (3.5%) over 500 stretching cycles with a peak strain of 10% (20%).

The benefit of a stable magnetic field sensitivity under a large mechanical strain is a result of the strain-relief structure in wrinkled SVRs. To well understand the strain-relief mechanism, we investigated the stretching behavior of the as-fabricated SVRs. Figure 5a depicts the local strains in the wrinkled SVRs. Releasing the tensile prestrain leads to a lateral elongation of the uncovered PDMS substrate due to the Poisson effect, while

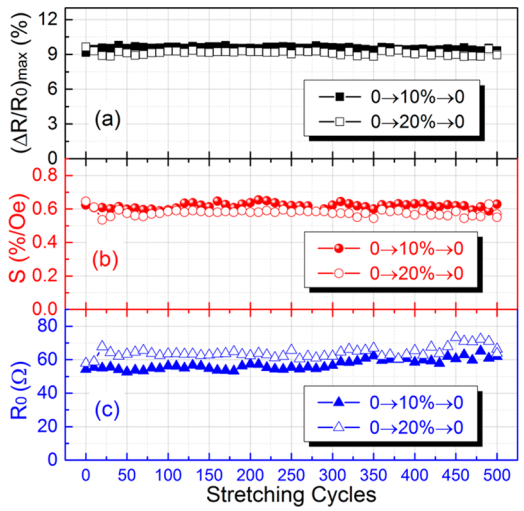

Figure 4. (a) The GMR ratio $(\Delta R/R_0)_{max}$ (squares), (b) magnetic field sensitivity S (circles), and (c) zero-field resistance R_0 (triangles) for the cyclic stretching tests of 0%−10%−0% (solid symbols) and 0%−20%−0% (open symbols) on the SVR-30%. The GMR curves were recorded every 10 stretching cycles at the maximum strain state. The test of $(0\%-20\%-0\%)_{500}$ was performed following the test of $(0\%-10\%-0\%)_{500}$ on the same piece of sample.

the width of metallic SVRs remains unchanged. This behavior is verified by the optical measurements shown in Figure 5b, indicating a negligible residual lateral strain in the as-fabricated SVRs. Obviously, the SVR ribbon/width ratio (W_{SVR}/W_{PDMS}) plays an important role in determining the stretchability of the SVRs. A peak force quantitative nanomechanical atomic force microscopy (PF-QNM AFM) characterization was performed to investigate the mechanical stability of the wrinkled SVRs grown with different W_{SVR}/W_{PDMS} and prestrains.[45−48] Note that the elastic modulus of PDMS in an ultrahigh strain state is no longer constant but parabolically increases as the applied strain increases.[49,50] For the SVR grown with the W_{SVR}/W_{PDMS} of 100 μm/200 μm and without the prestrain, the elastic modulus in PDMS measured in the Derjaguin−Muller−Toporov (DMT) model is constant and uniform (Figure 5c), suggesting there is no strain concentration in the uncovered PDMS area. However, as the tensile prestrain is increased to 50% (Figure 5d), the elastic modulus of PDMS gradually increases when approaching the SVR/PDMS boundary. For the sample in Figure 5e, the tensile prestrain keeps at 50%, but W_{SVR}/W_{PDMS} changes to 400 μm/200 μm. It is found that the elastic modulus of PDMS at the PDMS/SVR boundary is much higher than that in the central area, indicating an aggravated strain concentration at the SVR/PDMS boundary. Since the occurrence of cracks is determined by the strain-energy release rate that is proportional to ε_{PDMS}^2, the earliest cracking sites should be located at the PDMS/SVR boundaries.[49−51] When the lateral tensile strain in PDMS surpasses a critical value, a lot

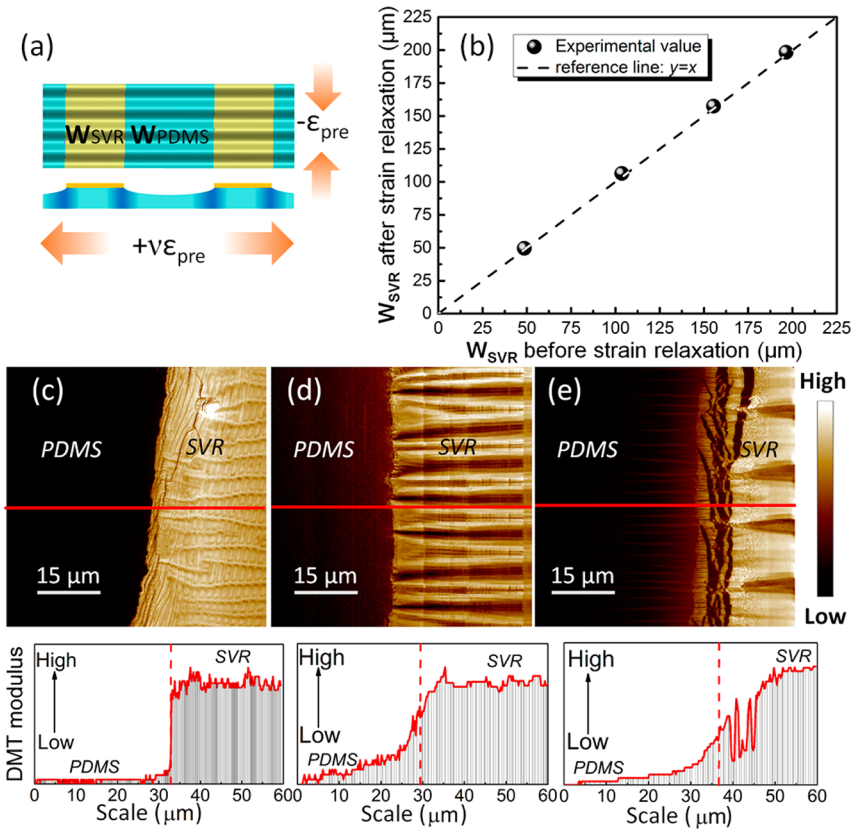

Figure 5. (a) A schematic configuration to illustrate the strain state in PDMS and SVRs after releasing the tensile prestrain. (b) The measured widths of a series of spin valve ribbons fabricated by different masks with different W_{SVR} and the fixed W_{PDMS} of 200 μm before and after releasing a tensile prestrain of 50%. The elastic modulus distributions (top) and the corresponding cross-sectional views (bottom, selected along the red lines) of the samples grown with (c) ε_{pre} = 0%, W_{SVR}/W_{PDMS} = 100 μm/200 μm, (d) ε_{pre} = 50%, W_{SVR}/W_{PDMS} = 100 μm/200 μm, and (e) ε_{pre} = 50%, W_{SVR}/W_{PDMS} = 400 μm/200 μm.

of microcracks are formed on the edge of the SVR (Figure 5e). To conclude, the mechanical stability of the strain-engineered SVRs is governed by the prestrain as well as the ribbon width ratio. Accordingly, in the experiment we designed the samples of SVR-30% and SVR-50% with the W_{SVR}/W_{PDMS} of 100 μm/200 μm, which are crack-resistant and highly stable under a large tensile strain.

CONCLUSION

In conclusion, we have employed a strain-relief structure for the fabrication of flexible spintronics devices by combining the periodic wrinkles and the parallel ribbons. Such a strain-engineered structure possesses a programmable stretchability up to a few tens of percent without fractures and obvious strain concentrations, thus ensuring a nondeteriorated magnetic field sensitivity and an excellent fatigue performance for the flexible spin valves. As compared to the previously reported flexible/stretchable magnetic sensors (Supporting Information, Table S1), our fabricated dual spin-valve sensor exhibits the nearly unchanged MR ratio of 9.9%, magnetic field sensitivity up to 0.69%/Oe, and zero-field resistance in a wide range of stretching strain. This kind of stretchable magnetic sensor is highly suitable for applications on a conformal shape or a movement part, such as smart skins or wearable electronics attached to body surfaces.

METHODS

Sylgard-184 poly(dimethylsiloxane) (PDMS)−30 vol % methylbenzene solution was magnetically stirred and spin-coated onto a commercial PDMS membrane to reduce its roughness. The PDMS precursor blend was cured in a vacuum oven at 70 °C overnight. The obtained PDMS substrate was 300 μm thick with a surface roughness of 0.33 nm (Supporting Information, Figure S1a). The PDMS substrate was prestretched and fixed on a homemade stretching apparatus (Supporting Information, Figure S1b). Then, the sputter deposition of the dual spin valve on prestretched PDMS substrate by using a band-like shadow mask (Figure 1b) was carried out in a 6-target ultrahigh-vacuum magnetron sputtering system. A couple of permanent magnets placed on the both sides of the substrates provided an in-plane magnetic field of 800 Oe during the sputtering deposition to induce an exchange bias perpendicular to the prestrain direction. Finally, after deposition, removing the shadow mask softly and releasing the prestrain resulted in wrinkled SVRs (Supporting Information, Figure S1c). The surface morphology was characterized by a Zeiss's confocal laser scanning microscope and a Bruker's multifunctional scanning probe microscope. The elastic modulus was measured by a PF-QNM AFM in the DMT model. To measure the GMR properties by 4-wire method, platinum wires with 30 μm in diameter were adhered to the wrinkled SVRs using high conductive silver paste and then heated at 70 °C on a hot plate for 2 h. Tensile strain was *in situ* applied through a homemade stretching apparatus with a micrometer screw gauge on it, which can modulate the tensile strain in a precise of 0.2%. In this experiment, the stretching of the SVR thin films covered under silver paste electrode was obviously confined. During the stretching measurements, the high concentration of strain around the electrodes caused the fractures in SVRs, resulting in an early failure of the devices before reaching the stretching limit.

ASSOCIATED CONTENT

Supporting Information

The Supporting Information is available free of charge on the ACS Publications website at DOI: 10.1021/acsnano.6b00034.

Additional experimental data (PDF)

AUTHOR INFORMATION

Corresponding Authors

*E-mail: zhanqf@nimte.ac.cn.

*E-mail: runweili@nimte.ac.cn.

Notes

The authors declare no competing financial interest.

ACKNOWLEDGMENTS

This work was supported by the National Natural Science Foundation of China (11374312, 11174302, 51401230, 51522105), the Instrument Developing Project of Chinese Academy of Sciences (YZ20132), and the China Postdoctoral Science Foundation (2014M560500).

REFERENCES

(1) Bauer, S. Sophisticated Skin. *Nat. Mater.* **2013**, *12*, 871−872.

(2) Bauer, S.; Bauer-Gogonea, S.; Graz, I.; Kaltenbrunner, M.; Keplinger, C.; Schwödiauer, R. A Soft Future: From Robots and Sensor Skin to Energy Harvesters. *Adv. Mater.* **2014**, *26*, 149−162.

(3) Hammock, M. L.; Chortos, A.; Tee, B. C.; Tok, J. B.; Bao, Z. The Evolution of Electronic Skin (E-Skin): A Brief History, Design Considerations, and Recent Progress. *Adv. Mater.* **2013**, *25*, 5997−6038.

(4) Huang, X.; Liu, Y.; Cheng, H.; Shin, W.-J.; Fan, J. A.; Liu, Z.; Lu, C.-J.; Kong, G.-W.; Chen, K.; Patnaik, D.; Lee, S.-H.; Hage-Ali, S.; Huang, Y.; Rogers, J. A. Materials and Designs for Wireless Epidermal Sensors of Hydration and Strain. *Adv. Funct. Mater.* **2014**, *24*, 3846−3854.

(5) Makarov, D.; Melzer, M.; Karnaushenko, D.; Schmidt, O. G. Shapeable Magnetoelectronics. *Appl. Phys. Rev.* **2016**, *3*, 011101.

(6) Chen, Y.-f.; Mei, Y.; Kaltofen, R.; Mönch, J. I.; Schumann, J.; Freudenberger, J.; Klauß, H.-J.; Schmidt, O. G. Towards Flexible Magnetoelectronics: Buffer-Enhanced and Mechanically Tunable GMR of Co/Cu Multilayers on Plastic Substrates. *Adv. Mater.* **2008**, *20*, 3224−3228.

(7) Melzer, M.; Makarov, D.; Calvimontes, A.; Karnaushenko, D.; Baunack, S.; Kaltofen, R.; Mei, Y.; Schmidt, O. G. Stretchable Magnetoelectronics. *Nano Lett.* **2011**, *11*, 2522−2526.

(8) Parkin, S. S. P. Flexible Giant magnetoresistance Sensors. *Appl. Phys. Lett.* **1996**, *69*, 3092−3094.

(9) Melzer, M.; Mönch, J. I.; Makarov, D.; Zabila, Y.; Cañón Bermúdez, G. S.; Karnaushenko, D.; Baunack, S.; Bahr, F.; Yan, C.; Kaltenbrunner, M.; Schmidt, O. G. Wearable Magnetic Field Sensors for Flexible Electronics. *Adv. Mater.* **2015**, *27*, 1274−1280.

(10) Karnaushenko, D.; Makarov, D.; Stober, M.; Karnaushenko, D. D.; Baunack, S.; Schmidt, O. G. High-Performance Magnetic Sensorics for Printable and Flexible Electronics. *Adv. Mater.* **2015**, *27*, 880−885.

(11) Karnaushenko, D.; Makarov, D.; Yan, C.; Streubel, R.; Schmidt, O. G. Printable Giant Magnetoresistive Devices. *Adv. Mater.* **2012**, *24*, 4518−4522.

(12) Melzer, M.; Karnaushenko, D.; Lin, G.; Baunack, S.; Makarov, D.; Schmidt, O. G. Direct Transfer of Magnetic Sensor Devices to Elastomeric Supports for Stretchable Electronics. *Adv. Mater.* **2015**, *27*, 1333−1338.

(13) Melzer, M.; Lin, G.; Makarov, D.; Schmidt, O. G. Stretchable Spin Valves on Elastomer Membranes by Predetermined Periodic Fracture and Random Wrinkling. *Adv. Mater.* **2012**, *24*, 6468−6472.

(14) Makarov, D.; Karnaushenko, D.; Schmidt, O. G. Printable Magnetoelectronics. *ChemPhysChem* **2013**, *14*, 1771−1776.

(15) Barraud, C.; Deranlot, C.; Seneor, P.; Mattana, R.; Dlubak, B.; Fusil, S.; Bouzehouane, K.; Deneuve, D.; Petroff, F.; Fert, A. Magnetoresistance in Magnetic Tunnel Junctions Grown on Flexible Organic Substrates. *Appl. Phys. Lett.* **2010**, *96*, 072502.

(16) Uhrmann, T.; Bär, L.; Dimopoulos, T.; Wiese, N.; Rührig, M.; Lechner, A. Magnetostrictive GMR Sensor on Flexible Polyimide Substrates. *J. Magn. Magn. Mater.* **2006**, *307*, 209−211.

(17) Lin, G.; Makarov, D.; Melzer, M.; Si, W.; Yan, C.; Schmidt, O. G. A highly Flexible and Compact Magnetoresistive Analytic Device. *Lab Chip* **2014**, *14*, 4050−4058.
(18) Meyners, D.; von Hofe, T.; Vieth, M.; Rührig, M.; Schmitt, S.; Quandt, E. Pressure Sensor Based on Magnetic Tunnel Junctions. *J. Appl. Phys.* **2009**, *105*, 07C914.
(19) Rong, J. H.; Yun, G. H.; Narsu, B.; Sprung, D. W. L. Ferromagnetic Resonance and Stress Anisotropy in Ferromagnetic/Antiferromagnetic Bilayer. *J. Appl. Phys.* **2006**, *100*, 083901.
(20) Xu, X.; Li, M.; Hu, J.; Dai, J.; Xia, W. Strain-Induced Magnetoresistance for Novel Strain Sensors. *J. Appl. Phys.* **2010**, *108*, 033916.
(21) Dokupil, S.; Bootsmann, M. T.; Stein, S.; Löhndorf, M.; Quandt, E. Positive/Negative Magnetostrictive GMR Trilayer Systems as Strain Gauges. *J. Magn. Magn. Mater.* **2005**, *290*−*291*, 795−799.
(22) Löhndorf, M.; Dokupil, S.; Bootsmann, M. T.; Malavé, A.; Rührig, M.; Bär, L.; Quandt, E. Characterization of Magnetostrictive TMR Pressure Sensors by MOKE. *J. Magn. Magn. Mater.* **2007**, *316*, e223−e225.
(23) Özkaya, B.; Saranu, S. R.; Mohanan, S.; Herr, U. Effects of Uniaxial Stresson the Magnetic Properties of Thin Films and GMR Sensors Prepared on Polyimide Substrates. *Phys. Status Solidi A* **2008**, *205*, 1876−1879.
(24) Pan, J.; Hu, J.-g. Ferromagnetic Resonance in Ferromagnetic/Antiferromagnetic Bilayers under the Stress Field. *Phys. Lett. A* **2006**, *358*, 236−241.
(25) Dai, G.; Zhan, Q.; Liu, Y.; Yang, H.; Zhang, X.; Chen, B.; Li, R.-W. Mechanically Tunable Magnetic Properties of $Fe_{81}Ga_{19}$ films Grown on Flexible Substrates. *Appl. Phys. Lett.* **2012**, *100*, 122407.
(26) Zhang, X.; Zhan, Q.; Dai, G.; Liu, Y.; Zuo, Z.; Yang, H.; Chen, B.; Li, R.-W. Effect of Mechanical Strain on Magnetic Properties of Flexible Exchange Biased FeGa/IrMn Heterostructures. *Appl. Phys. Lett.* **2013**, *102*, 022412.
(27) Liu, Y.; Zhan, Q.; Dai, G.; Zhang, X.; Wang, B.; Liu, G.; Zuo, Z.; Rong, X.; Yang, H.; Zhu, X.; Xie, Y.; Chen, B.; Li, R.-W. Thermally Assisted Electric Field Control of Magnetism in Flexible Multiferroic Heterostructures. *Sci. Rep.* **2014**, *4*, 6925.
(28) Cerda, E.; Mahadevan, L. Geometry and Physics of Wrinkling. *Phys. Rev. Lett.* **2003**, *90*, 074302.
(29) Efimenko, K.; Rackaitis, M.; Manias, E.; Vaziri, A.; Mahadevan, L.; Genzer, J. Nested Self-Similar Wrinkling Patterns in Skins. *Nat. Mater.* **2005**, *4*, 293−297.
(30) Khang, D. Y.; Jiang, H.; Huang, Y.; Rogers, J. A. A Stretchable Form of Single-Crystal Silicon for High-Performance Electronics on Rubber Substrates. *Science* **2006**, *311*, 208−212.
(31) Jiang, H.; Khang, D. Y.; Song, J.; Sun, Y.; Huang, Y.; Rogers, J. A. Finite Deformation Mechanics in Buckled Thin Films on Compliant Supports. *Proc. Natl. Acad. Sci. U. S. A.* **2007**, *104*, 15607−15612.
(32) Kim, D. H.; Ahn, J. H.; Choi, W. M.; Kim, H. S.; Kim, T. H.; Song, J.; Huang, Y. Y.; Liu, Z.; Lu, C.; Rogers, J. A. Stretchable and Foldable Silicon Integrated Circuits. *Science* **2008**, *320*, 507−511.
(33) Kaltenbrunner, M.; Sekitani, T.; Reeder, J.; Yokota, T.; Kuribara, K.; Tokuhara, T.; Drack, M.; Schwödiauer, R.; Graz, I.; Bauer-Gogonea, S.; Bauer, S.; Someya, T. An Ultra-Lightweight Design for Imperceptible Plastic Electronics. *Nature* **2013**, *499*, 458−463.
(34) White, M. S.; Kaltenbrunner, M.; Głowacki, E. D.; Gutnichenko, K.; Kettlgruber, G.; Graz, I.; Aazou, S.; Ulbricht, C.; Egbe, D. A. M.; Miron, M. C.; Major, Z.; Scharber, M. C.; Sekitani, T.; Someya, T.; Bauer, S.; Sariciftci, N. S. Ultrathin, Highly Flexible and Stretchable PLEDs. *Nat. Photonics* **2013**, *7*, 811−816.
(35) Li, X.; Gu, T.; Wei, B. Dynamic and Galvanic Stability of Stretchable Supercapacitors. *Nano Lett.* **2012**, *12*, 6366−6371.
(36) Um, D. S.; Lim, S.; Lee, Y.; Lee, H.; Kim, H. J.; Yen, W. C.; Chueh, Y. L.; Ko, H. Vacuum-Induced Wrinkle Arrays of InGaAs Semiconductor Nanomembranes on Polydimethylsiloxane Microwell Arrays. *ACS Nano* **2014**, *8*, 3080−3087.
(37) Melzer, M.; Kaltenbrunner, M.; Makarov, D.; Karnaushenko, D.; Karnaushenko, D.; Sekitani, T.; Someya, T.; Schmidt, O. G. Imperceptible Magnetoelectronics. *Nat. Commun.* **2015**, *6*, 6080.
(38) Anderson, G.; Huai, Y. M.; Miloslawsky, L. CoFe/IrMn Exchange Biased Top, Bottom, and Dual Spin Valves. *J. Appl. Phys.* **2000**, *87*, 6989−6991.
(39) Tong, H.-C.; Liu, F.; Stoev, K.; Chen, Y.; Shi, X.; Qian, C. The Dual Spin Valve Head for High Density Recording. *J. Magn. Magn. Mater.* **2002**, *239*, 106−111.
(40) Law, R.; Sbiaa, R.; Liew, T.; Chong, T. C. Magnetoresistance and Switching Properties of Co−Fe/Pd-Based Perpendicular Anisotropy Single- and Dual-Spin Valves. *IEEE Trans. Magn.* **2008**, *44*, 2612−2615.
(41) Chun, B. S.; Fowley, C.; Abid, M.; Coey, J. M. D. Three-State Dual Spin Valve Structure. *J. Phys. D: Appl. Phys.* **2010**, *43*, 025002.
(42) Lacour, S. P.; Wagner, S.; Huang, Z.; Suo, Z. Stretchable Gold Conductors on Elastomeric Substrates. *Appl. Phys. Lett.* **2003**, *82*, 2404−2406.
(43) Chen, X.; Hutchinson, J. W. Herringbone Buckling Patterns of Compressed Thin Films on Compliant Substrates. *J. Appl. Mech.* **2004**, *71*, 597−603.
(44) Huang, Z. Y.; Hong, W.; Suo, Z. Nonlinear Analyses of Wrinkles in a Film Bonded to a Compliant Substrate. *J. Mech. Phys. Solids* **2005**, *53*, 2101−2118.
(45) Young, T. J.; Monclus, M. A.; Burnett, T. L.; Broughton, W. R.; Ogin, S. L.; Smith, P. A. The Use of the PeakForce Quantitative Nanomechanical Mapping AFM-Based Method for High-Resolution Young's Modulus Measurement of Polymers. *Meas. Sci. Technol.* **2011**, *22*, 125703.
(46) Li, T.; Suo, Z. Deformability of Thin Metal Films on Elastomer Substrates. *Int. J. Solids Struct.* **2006**, *43*, 2351−2363.
(47) Derjaguin, B. V.; Muller, V. M.; Toporov, Y. P. Effect of Contact Deformations on the Adhesion of Particles. *J. Colloid Interface Sci.* **1975**, *53*, 314−326.
(48) Maugis, D. Adhesion of Spheres: The JKR-DMT Transition Using a Dugdale Model. *J. Colloid Interface Sci.* **1992**, *150*, 243−269.
(49) Chen, Z.; Cotterell, B.; Wang, W. The fracture of Brittle Thin Films on Compliant Substrates in Flexible Displays. *Eng. Fract. Mech.* **2002**, *69*, 597−603.
(50) Olliges, S.; Gruber, P. A.; Orso, S.; Auzelyte, V.; Ekinci, Y.; Solak, H. H.; Spolenak, R. *In situ* Observation of Cracks in Gold Nano-Interconnects on Flexible Substrates. *Scr. Mater.* **2008**, *58*, 175−178.
(51) Chen, Z.; Cotterell, B.; Wang, W.; Guenther, E.; Chua, S.-J. A Mechanical Assessment of Flexible Optoelectronic Devices. *Thin Solid Films* **2001**, *394*, 201−205.